# Control of intermetallic nano-particles through annealing in duplex low density steel

Alireza Rahnama, Stephen Spooner, Seetharaman Sridhar


www.elsevier.com

PII: S0167-577X(16)31759-1
DOI: http://dx.doi.org/10.1016/j.matlet.2016.11.020
Reference: MLBLUE21714

To appear in: *Materials Letters*

Received date: 1 July 2016
Revised date: 10 October 2016
Accepted date: 5 November 2016

Cite this article as: Alireza Rahnama, Stephen Spooner and Seetharaman Sridhar Control of intermetallic nano-particles through annealing in duplex low density steel, *Materials Letters,* http://dx.doi.org/10.1016/j.matlet.2016.11.020

# Control of intermetallic nano-particles through annealing in duplex low density steel

Alireza Rahnama[☆], Stephen Spooner, Seetharaman Sridhar

*Internationational Digital Laboratory, Warwick Manufacturing Group, University of Warwick, Coventry, United Kingdom, CV4 7AL*

**Abstract**

In high Al-low-density steels for future vehicle light weighting, it is vital to design a thermal profile to form and retain the uniformly dispersed nanosize B2-type intermetallic precipitates that are crucial for the material strength. In this paper, the influence of heating rate, during annealing to $1050°\mathrm{C}$ was simulated in a Au-image furnace. The post annealing structure was then characterized and two different morphologies of B2 particles were observed: triangle-like with a few micrometres and disk-like precipitates with a diameter of around a few hundred nanometres. It was found that a slower heating rate ($2.5°\mathrm{C/s}$) led to an increase in the volume fraction and to uniform distribution of particles within the microstructure and considerably affected the shape and size of the precipitates.

*Keywords:* Low density steel, Intermetallic, Heat treatment, Mechanical properties

*2010 MSC:* 00-01, 99-00



Lightweight steels with excellent combinations of specific strength and ductility have attracted considerable attention recently [1, 2, 3, 4]. Lightweight steels are often heavily alloyed leading to a usually complex microstructure, consisting of multiple phases and ordered intermetallic compounds. Duplex low density steels (Al 7-10 wt.%, Mn 5-15 wt.%, C 0.4-0.9 wt.%) can usually provide better combination of strength and ductility in comparison with ferritic or austenitic steels [1, 2, 3, 4] but it is critical to

☆Fully documented templates are available in the elsarticle package on CTAN.
☆Corresponding author: Alireza Rahnama, Email address: a.rahnama@warwick.ac.uk

control the various ordered phases which are formed depending on the processing conditions and composition to achieve the required strength. This includes the $L1_2$-type $\kappa$ phase, the CsCl-type B2 phase, and the $F_{m3m}$-type $DO_3$ phase [1, 2, 3, 5, 6, 7, 8]. Recently, Kim et. al. [9] showed that hard intermetallic compounds can be effectively used as a strengthening second phase in high Al low density steel, while reducing its harmful effect on ductility by controlling its morphology and dispersion. In such a microstructure, B2 particles are responsible for the high work hardening rate due to their non-shearable nature [10], while the austenite phase provides the favourable ductility. In this way, a microstructure was designed which has a combination of specific strength and ductility. However, there was no information provided by the authors on the thermal cycle that was employed in this study to form such a uniform microstructure. From a practical point of view, the ability to control the size, volume fraction, morphology and uniform distribution of B2-type intermetallic is the key to understand the mechanical properties of this type of lightweight steels. In order to control these factors, it is critical to design a thermal profile to precipitate and preserve the nano-sized intermetallic precipitates that are crucial for the strength. It was, therefore, the objective of the current work to study the influence of heating rate, during annealing to $1050°C$, on the size, volume fraction, morphology and dispersion of B2-type intermetallic in a duplex low density steel.

The steel in this work had a composition (in wt.%) of 0.8C- Al-15 Mn-5 Ni. The hot-rolled material was first solution-treated for 35 min at $1250°C$ in a Au-furnace under Ar, and then water-quenched. The heat treated samples was prepared with dimensions of 3-mm (length), 3-mm (width) and 1-mm (thickness). The microstructure at ambient temperature was coarse-grain austenite ($>10\ \mu m$) and elongated, coarse-grained ferrite. The subsequent annealing treatments were performed at $1050°C$ for 5 minutes at three different heating rates: $2.5°\mathrm{C/s}$, $5°\mathrm{C/s}$ and $7.5°\mathrm{C/s}$. One sample was also heat treated at a heating rate of $2.5°\mathrm{C/s}$ up to $550°C$ and without holding, cooled down to room temperature ($50°\mathrm{C/min}$) (interrupted experiment sample, IES). This was done in order to investigate if there was any other ordering mechanisms occurring during the heating of the samples to the higher temperature. $1050°C$ was chosen as the annealing temperature, because B2 is the only thermodynamically stable phase,

among the three precipitations discussed above, at this temperature [10]. Five minutes was chosen as the isothermal time to avoid the formation of coarse particles which are detrimental to mechanical properties. The microstructure of the samples was characterized by Carl Zeiss Sigma FE-SEM) and JEOL 2000FX TEM. The Vickers hardness was measured using a Buehler Tukon 1102 micro hardness tester employing 100 g load for a dwell time of 10 s.

Fig. 1a1-4 shows the EBSD maps of the samples under study. The initial microstructure consists of austenite and ferrite (Fig. 1a1). Fig.1a2 shows the microstructure of the sample heated at $2.5^{\circ}\mathrm{C/s}$. As is evident from this figure, several precipitates formed both at $\gamma - \gamma$ grain boundaries and within the $\gamma$ grains ($\mathrm{B2}_{\gamma}$). EDS examinations of all the heat treated samples shows that Al and Ni are enriched in the B2-type particles as well as in the elongated phase (initially ferrite), while the Fe and Mn are is enriched in austenite $(\gamma)$. The enrichment of Ni and Al in what was originally ferrite indicates the formation of B2-type Ni-Al intermetallic compounds in this phase. The composition of the precipitates obtained by EDX analysis was 26.6 Al-6.9 Mn-15.6 Ni-51.3 Fe (wt%). The measured Al and Ni contents of B2 was higher compared with that reported by Kim et al. [9] as the annealing temperature employed in this study was higher. The microstructure of the sample heat treated at $5^{\circ}\mathrm{C/s}$ is shown in Fig.1a3. The number of $\mathrm{B2}_{\gamma}$ precipitates within the $\gamma$ grains decreased in comparison to the sample heated at $2.5^{\circ}\mathrm{C/s}$. However, the number of grain boundary (GB) precipitates at the $\gamma - \gamma$ boundaries remained unchanged. For sample heat treated at $7.5^{\circ}\mathrm{C/s}$, precipitates were absent in the grain interior and only precipitated at $\gamma - \gamma$ grain boundaries as shown in Fig.1a4. As is evident from Fig.1a2-4, the most uniform microstructure of B2 particles was achieved by heating rate of $2.5^{\circ}\mathrm{C/s}$.

The volume fraction of BCC structure (red phase, $V_{(\alpha+B2_{\gamma})}$) as well as that of disk-like $\mathrm{B2}_{\alpha}$ particles ($V_{B2_{\alpha}}$) were found to decrease with increasing heating rate due to reduced ordering time available for the formation of the B2 structure. Moreover, the length and width of the elongated BCC structure decreased with heating rate (Table. 1). The bright-field micrographs of these precipitates of the sample annealed with a heating rate of $2.5^{\circ}C/s$ are shown in Fig. 1b and c. Two different morphologies of the B2-type intermetallic were found: B2 with flat interfaces and sharp edges with an

average size of a $\simeq 1.4\ \mu m$ formed in the $\gamma$ phase ($B2_\gamma$), and disk-like precipitates with a size of a few hundred nanometres formed in $\alpha$ matrix ($B2_\alpha$). The disk-like nanosize B2 particles precipitated in $\alpha$ was not reported in the Ref.[9]. For the sample heat treated at $2.5°C/s$, disk-like B2-type particles were formed and uniformly distributed within the $\alpha$ phase (Fig. 1c). The uniform distribution of particles was not observed under TEM for the samples heat treated at $5°C/s$ and $7.5°C/s$.

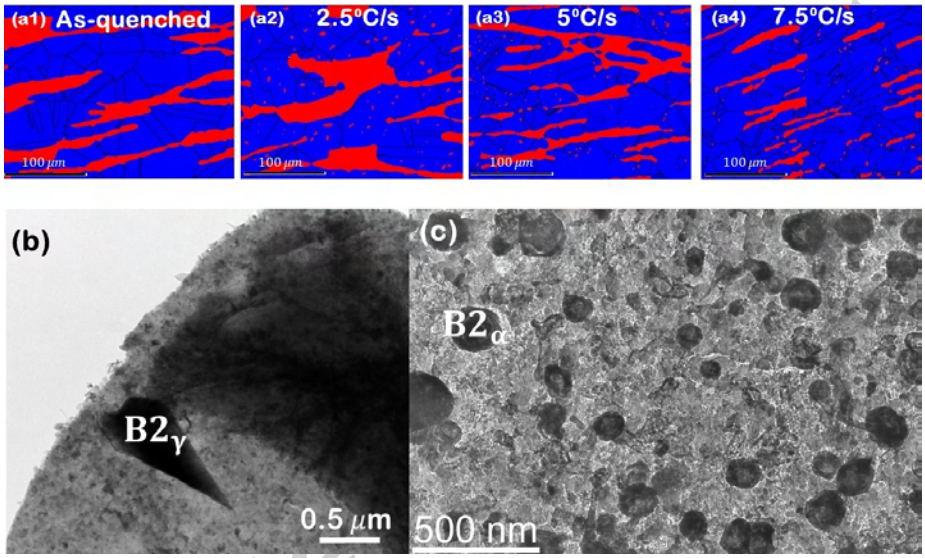


Figure 1: The EBSD maps of (a1) as-quenched sample, and the samples heat treated at (a2) $2.5°C/s$, (a3) $5°C/s$ and (a4) $7.5°C/s$ (in all EBSD maps, the red phase corresponds to BCC structure while the blue phase is FCC structure.) (b) Triangle-like B2 precipitate in $\gamma$ and (c) disk-like B2 particles in the $\alpha$ phase. Both (b) and (c) were taken from the sample annealed with a heating rate of 2.5.

Fig. 2 shows the x-ray diffraction (XRD) profiles of the steel heat treated under different conditions - only the peaks of the ordered phases that do not overlap with those of the matrix are indicated. In the as-quenched state, no peaks associated with ordered phases were found. The $31°$ peak corresponds to (222)$DO_3$ or (100)B2 and the $55°$ peak corresponds to (222) $DO_3$ or (111) B2. However, no peaks corresponding to $\kappa$ phase, $2\theta = 34°$ for $(110)_\kappa$ and $75°$ for $(300)_\kappa$ were found. The peaks of ordered phase became stronger for the samples treated at $1050°$. However, as indicated by arrows, the peaks of (311)$DO_3$ at $2\theta = 52°$, which were clearly visible for IES, disappeared by $1050°$ ordering. Therefore, the peaks at $2\theta = 31°$ and $55°$ in the XRD profile at $1050°$

correspond to (100) B2 and (111) B2, respectively.

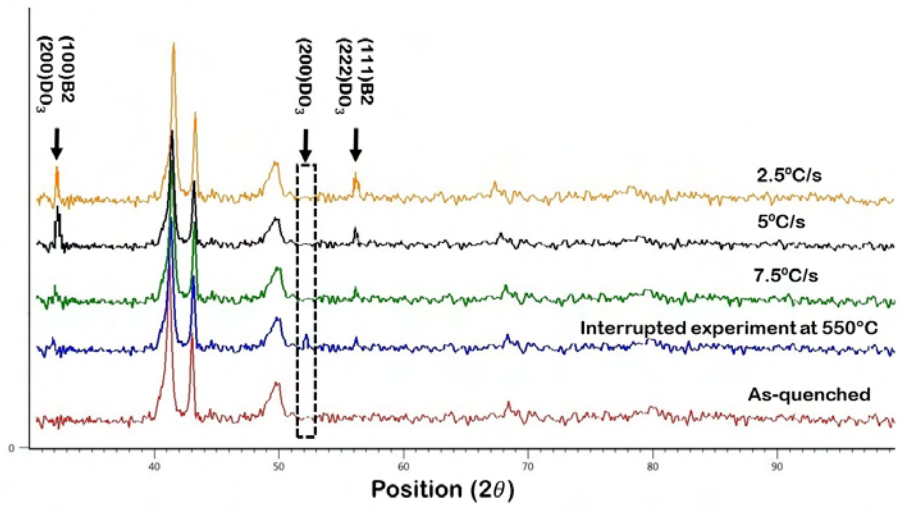


Figure 2: XRD profiles of the as-quenched, IES, and samples heat treated at $1050°C$ with heating rates of $2.5°C/s$, $5°C/s$ and $7.5°C/s$. Only the peaks of the ordered phases that are not overlapped with the matrix phases are labelled.

Table. 1 shows the hardness values for the as-quenched, IES, and the samples heat treated at $2.5°C/s$, $5°C/s$ and $7.5°C/s$. The hardness of IES was higher than that of the as-quenched sample. The matrix phase fraction of both steels was expected to be comparable because of the short ordering time. In addition, no $\kappa$-carbide was found in $\gamma$. Accordingly, the higher strength of the IES is anticipated to be originated from strengthening in ferrite. Despite the existence of a substantial amount of disordered ferrite, ferrite of IES was believed to mainly consist of $DO_3$ domains rather than a Fe-solution phase. This was supported by the XRD profile of IES. Park [11] investigated the effects of the ordering temperature on room temperature yield strength (YS) of a hypostoichiometric Fe-24.1Al (in at.%) intermetallic and it was found that the Fe-24.1Al exhibited the disordered ($\alpha + DO_3$) region at $450°C$ to $550°C$ and the B2 single phase region at $580°C$ to $720°C$. The YS showed a maximum peak around $500°C$ corresponding to where ($\alpha + DO_3$) is stable. The YS decreased in the B2 region. Marcinkowski and Leamy [12] reported that the nucleation energy of superdislocation loops in the $DO_3$ superlattice is higher than that in B2 superlattice. This

leads to the higher stress for superdislocation generation in the former, leading to the higher YS. $DO_3$ strengthening is, thus, believed to be reason for the higher strength of the $\alpha$ phase of IES in comparison with that of the as-quenched sample. However, the measured hardness value of the $\alpha$ phase of IES was remarkably less than that for the sample heat treated at $5°C/s$ and in particular for the sample heat treated at $2.5°C/s$. Breuer et al. conducted a series of experiment and measured the enthalpy of formation of $B2-Fe_{1-x}-Al_x$ and $B2-(Fe,Ni)_{1-x}-Al_x$ at 1073K. Their results showed that generally enthalpy of formation of $B2-(Fe,Ni)_{1-x}-Al_x$ is of greater magnitude than that of $B2-Fe_{1-x}-Al_x$. It was also shown that starting with binary $B2-Fe_{1-x}-Al_x$ and replacing Fe with Ni, $B2-(Fe,Ni)_{1-x}Al_x$ while keeping the Al content at a constant value, the enthalpy of formation becomes increasingly more negative [13]. The EDX analysis of B2-type precipitates for all three samples heat treated at $2.5°C/s$, $5°C/s$ and $7.5°C/s$, showed the Ni content in the precipitates is higher than the $\alpha + DO_3$ of IES (18.9 Al-7.5 Mn-10.1 Ni-63.5 Fe all in wt.%). Therefore, it was anticipated that the increased hardness values of $\alpha$ phases for the samples heat treated at $2.5°C/s$ and $5°C/s$ in comparison with IES is due to the stronger Ni-Al bonds in comparison to Fe-Al bonds. The hardness values of both $\alpha$ and $\gamma$ phases increased with decreasing heating rate. This was believed to be due to the increase in the volume fractions of $B2_\alpha$ and $B2_\gamma$ with decreasing heating rate. In addition, the average diameter of $B2_\alpha$ was determined to be: $170.1 \pm 7$ nm for sample heat treated at $2.5°C/s$, $174.4 \pm 5$ nm for sample heat treated at $5°C/s$ and $111.4 \pm 3$ for sample heat treated at $7.5°C/s$. Although the dispersion of particles in $\gamma$ phase for three heat treated samples was different, no significant variation in the average size of $B2_\gamma$ particles was observed.

Table 1: The variation in length and width of as-quenched, and samples heat treated at $2.5°C/s$, $5°C/s$ and $7.5°C/s$. For each sample, 50 randomly selected fields at a magnification of $\times 100$ in the SEM were considered. The hardness values for both $\alpha$ and $\gamma$ for each aforementioned samples as well as IES are also shown.

| Condition | Length ($\mu m$)($bcc_\alpha$) | Width ($\mu m$) ($bcc_\alpha$) | Average diameter of $B2_\alpha$ (nm) | Hardness of $\alpha$ phase ($HV_{0.1}$) | Hardness of $\gamma$ phase ($HV_{0.1}$) | $V_{(\alpha+B2_\alpha)}$ (%) | $V_{B2_\alpha}$ (%) | location of precipitates in $\gamma$ | uniform dispersion of particles |
|---|---|---|---|---|---|---|---|---|---|
| As-quenched | $423 \pm 10$ | $22 \pm 10$ | - | 321 | 385 | - | - | - | - |
| IES | - | - | - | 351 | 386 | - | - | - | - |
| Sample heat treated at $2.5°C/s$ | $346 \pm 8$ | $31 \pm 7$ | $170.1 \pm 7$ | 388 | 492 | 31.7 | 35.4 | GB and grains interior | Yes |
| Sample heat treated at $5°C/s$ | $237 \pm 13$ | $18 \pm 11$ | $174.4 \pm 5$ | 372 | 407 | 24.4 | 21.1 | Mostly GB | No |
| Sample heat treated at $7.5°C/s$ | $94 \pm 7$ | $11 \pm 3$ | $111.4 \pm 3$ | 363 | 392 | 20.1 | 4.2 | Only GB | No |

In summary, we observed two different morphologies of B2 precipitates, coarse

particles with flat sides and sharp edges in $\gamma$ along with nanosize disk-like particles in $\alpha$. Slower heating rate led to an even distribution of B2 precipitates in the $\gamma$ matrix ($B2_\gamma$) and of the disk-like precipitates within the $\alpha$ phase ($B2_\alpha$). The coarse $B2_\gamma$ precipitates located in the austenite grains or grain-boundaries. EDX analysis was performed and the composition of B2-intermetallics formed at $1050°C$ was determined to be Fe-26.6 Al-6.9 Mn-15.6 Ni (all in wt.%). It was found that increasing the heating rate resulted in a decrease in the volume fraction of $B2_\gamma$ and $B2_\alpha$ particles as well as in the length and width of the elongated BCC $\alpha$ phase in Fe-0.8C-15Mn-10Al-5Ni. It was also found that the B2 intermetallics form a harder structure than $DO_3$ in the presence of Ni owing to the strong Ni-Al bonds.

**Acknowledgement**

Financial assistance from the WMG Centre High Value Manufacturing Catapult with focus on low C mobility is gratefully acknowledged. The authors gratefully thank Dr. Arunansu Halder and Dr. Shangping Chen who provided insight and expertise that greatly assisted the research.

**Contribution**

A. Rahnama and S. Sridhar designed the study; A. Rahnama performed the research; A. Rahnama and S. Sridhar analysed the data; and A. Rahnama, S. Spooner and S. Sridhar wrote the paper. All authors commented on the manuscript.

**References**

[1] Rana R, Liu C, Ray RK. Scr Mater 2013;68:354-9.

[2] Sohn SS, Song H, Suh BC, Kwak JH, Lee BJ, Kim NJ, Lee S, Acta Mater 2015;96:301-10.

[3] Gutierrez-Urrutia I, Raabe D. Scr Mater 2013;68:343-7.

[4] Seol JB, Raabe D, Choi P, Park HS, Kwak JH, Park CG. Scr Mater 2013;68:348-53.

[5] Sutou Y, Kamiya N, Umino R, Ohnuma L, Ishida L, ISIJ Int 2010; 50:680-6.

[6] Heo YU, App. Microscopy 2014; 44:144.

[7] Kerl R, Wolff J, Hehenkamp Th. Intermetallics 1999;7:301.

[8] Rahnama A, Dashwood R, Sridhar S, Comp. Mater. Sci 2017; 126: 152-159.

[9] Kim SH, Kim H, Kim NJ. Nature 2015; 518:77-9.

[10] Frommeyer G, Brux U, Steel Res Int 2006; 77:627-33.

[11] Park JW, Intermetallics 2002; 10:683.

[12] Marcinkowski MJ, Brown N, Fisher RM. Acta Metall. 1961; 9:129.

[13] Bruer J, Grun A, Sommer F, Mittemeijer EJ. Metal. Mater. Trans. B 2001; 32B:913.